# Energetic particle physics issues for three-dimensional toroidal configurations

D. A. Spong[1)], Y. Todo[2)], M. Osakabe[2)], L. Berry[1)], B. N. Breizman[3)], D.L. Brower[4)], C. B. Deng[4)], A. Konies[5)]
[1)] Oak Ridge National Laboratory, USA
[2)] National Institute for Fusion Science, Japan
[3)] Institute for Fusion Studies, The University of Texas, Austin, Texas, USA
[4)] Department of Physics, University of California, Los Angeles, CA, USA
[5)] Max-Planck Institut für Plasmaphysik, EURATOM-Association, Greifswald, Germany

E-mail contact of main author: spongda@ornl.gov

**Abstract.** Energetic particle physics issues are of significant interest in stellarators and rippled tokamaks. The existence and stability of shear Alfvén (SA) modes in stellarators have been examined computationally through a sequence of continuum, discrete eigenmode and δf calculations. Although 3D couplings greatly increase the number of available SA modes, many of these are continuum damped. By identifying the more viable modes good contact has been made with experimental observations of TAE instabilities on LHD. Sound-wave or parallel compressibility couplings can modify the Alfvén spectrum at low frequencies and have been incorporated into the STELLGAP code. Regions with coupled SA-sound continua are found in frequency ranges on the HSX experiment where coherent mode activity is observed. Finally, symmetry breaking effects are studied in ITER, taking into account TF ripple, ferritic inserts and tritium blanket modules. Finite β 3D equilibria are obtained, indicating that ripple is amplified within the plasma by the self-consistent currents over vacuum levels.

## 1. Introduction

Toroidal magnetic confinement devices can be three-dimensional either by design (stellarators) in order to create external rotational transform and accomplish other physics goals or by necessity (tokamaks), due to discrete toroidal field coils, ferritic steel tritium breeding blanket modules, and various symmetry-breaking control coils required for resistive wall modes and ELM mitigation. However, three-dimensional variations in the confining magnetic field have consequences for energetic particle populations such as neutral beam ions, RF minority populations and fusion-produced alpha particles. Good single particle confinement is only assured if there is symmetry, leading to a conserved canonical momentum and bounded deviations of the orbit trajectory from flux surfaces. Likewise, the potential for fast particle destabilization of MHD modes is influenced by magnetic symmetry. For example, the discrete shear Alfvén gap mode density is minimal in a cylinder where two symmetry directions exist (i.e., only GAE modes would be present in a cylinder). For configurations with one symmetry direction (axisymmetric tokamak), the gaps driven by poloidal mode couplings (TAE, EAE, NAE) become available. Finally, for devices (stellarators) that have no axial symmetry, an additional set of gaps driven by toroidal and helical mode couplings (MAE, HAE) are present.

In this paper, several energetic particle physics issues for three-dimensional configurations will be presented and analyzed. First, the shear Alfvén spectrum and methods for selecting modes prone to destabilization will be described along with recently developed computational tools. Next, the sound wave coupling will be included and its impact on low frequency Alfvén modes analyzed, in particular for the case of low shear stellarators, where the GAE and sound wave can coexist. Finally, a self-consistent equilibrium analysis of field ripple effects in ITER will be described, which includes discrete TF ripple, ferritic inserts, and low field period perturbations from non-symmetrically distributed tritium blanket modules and indicates the

ripple amplification effects of the Shafranov shift, finite β diamagnetic currents and Pfirsch-Schlüter flows.

## 2. Shear Alfvén spectrum and instabilities in stellarators

Energetic particle destabilized coherent modes have been observed in nearly all stellarator experiments, beginning in 1994 with W7-AS [1] and extending to CHS [2], LHD [3], TJ-II [4], Heliotron-J [5] and HSX [6]. A wide phenomenology of Alfvén mode activity has been identified, including GAE, TAE, HAE, EPM and RSAE modes. Both regimes with benign effects on fast particle confinement have been seen, as well as those with enhanced losses. In order to better interpret the experimental results methods have been developed to calculate the Alfvén continuum [15] (STELLGAP code) and discrete mode structure [7] (AE3D code), taking into account the 3D equilibrium. Calculations of Alfvén modes in stellarators have also been done with the CAS3D code [8] that include compressibility couplings.

Alfvén continuum results from the STELLGAP code are shown in Fig. 1(a) for an LHD discharge (#47645) [9] where Alfvénic activity was observed. In Fig. 1(b) and 1(c) results from the AE3D (Alfvén mode structure) code are shown for this same case. These results are based on taking a central density of $1 \times 10^{20}$ $m^{-3}$ and hydrogen ions. AE3D solves for all of the shear Alfvén eigenmodes present in Eq. (1), which is derived in the reduced MHD limit; the mode structure is represented using finite elements in the flux surface coordinate and Fourier expansions in poloidal/toroidal angles. Normally, all of the eigenvalues are of interest, but much higher performance is possible by using a Jacobi-Davidson algorithm that calculates a cluster of about 40 eigenvalues centered on a specified input frequency.

$$\omega^2 \nabla \bullet \left( v_A^{-2} \nabla \phi \right) = \mathbf{B} \bullet \nabla \left[ \frac{1}{B} \nabla^2 \left( \frac{\mathbf{B}}{B} \bullet \nabla \phi \right) \right] \qquad (1)$$

In Fig. 1(b) the volume integrated (normalized) electrostatic energy: $E_s = C_0 \int d^3x \left( \nabla_\perp \phi \bullet \nabla_\perp \phi \right) / v_A^2$ is plotted vs. frequency for eigenmodes found by AE3D up to 600 kHz, while Fig. 1(c) shows the density of modes vs. frequency. Here the normalization $C_0$ is chosen for each eigenmode so that the peak value of the largest Fourier component, $\phi_{mn}(\rho)$ is 1. The energy and mode density are measures that have been found useful for identifying modes that less subject to continuum damping. As Fig. 1(b) shows, the electrostatic energy of these eigenmodes varies significantly. The modes with the higher energies are generally those with strong continuum interactions since strong gradient regions in their radial structure are associated with continuum crossings. As can be seen, stellarators have a very large collection of Alfvén modes present; this is due to the toroidal mode couplings driven by the N-fold symmetric equilibrium. For stellarators, toroidal mode families must be considered while for tokamaks only a single n need be considered. For the results in Fig. 1, the n = 1 mode family was used with couplings taken into account with n = -11, -9, -1, 9 and 11. As the radial and spectral resolution is increased, the number of Alfvénic eigenmodes grows and sorting through them to find experimentally relevant modes becomes an increasing challenge. Most of these modes are continuum modes, i.e., modes whose frequency intersects nearby Alfvén continua, and thus would be expected to be strongly damped. On this basis, the lower energy modes are of most interest and as Fig. 1(b) shows, there are clumps of low energy modes present at frequencies corresponding to the more open continuum gap regions. The eigenmode density also typically shows large drops near open gap regions, as is apparent in the 50-60 kHz range. These two measures (averaged mode energy and density) may be useful

target functions in optimizing future stellarators to minimize Alfvén instabilities. In the case of the eigenmode density, there are more efficient linear algebra methods available that do not require solving directly for all of the eigenmodes.

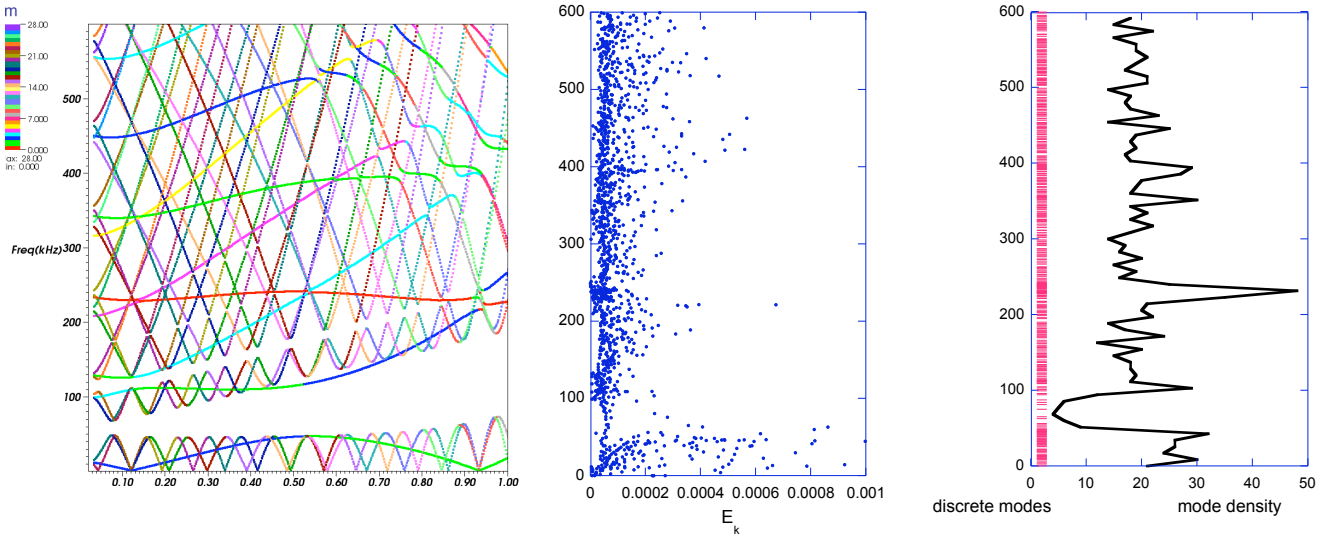


*Figure 1 – (a) shear Alfvén continua for n = 1 mode family in LHD; (b) volume averaged normalized electrostatic energy for Alfvén eigenmodes present in (a); eigenmode density vs. frequency.*

Based on these considerations, and inspecting mode structures, it is possible to find modes in the lower TAE gap with global radial mode structures that do not show strong continuum interactions. The radial structure of one such mode at 55 kHz is shown in Fig. 2(a) and its 3D variation on a flux surface is given in Fig. 2(b). Coherent mode activity in this frequency range was measured in LHD discharge #47645 [9] and has been related to formation of phase space island structures [10] that lead to rapid fast ion transport over about 10% of the plasma radius.

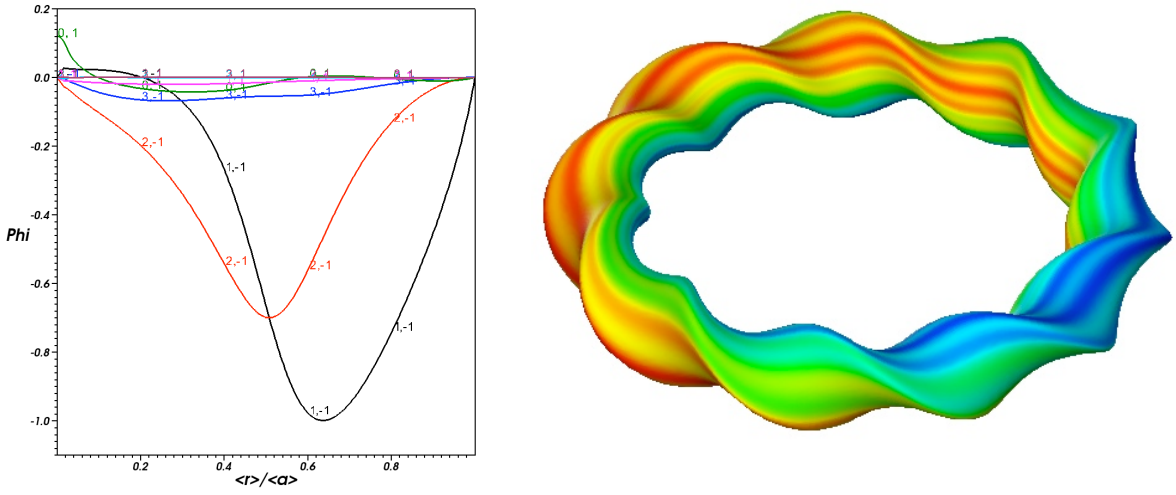


*Figure 2 – (a) Radial mode structure for a global TAE mode found in the lower open gap of Figure 1(a); (b) 3D variation of this mode on the outer flux surface of LHD.*

A new method for evaluating the stability of these modes has recently been developed as an extension to the AE3D calculation. This is done in the time domain using the δf method and

follows a large collection of unperturbed marker particle orbits in the presence of an Alfvén mode structure. This is a perturbative technique, but it allows finite orbit width effects to be retained in a natural way. Stability and linear growth rates can then be assessed from the ensemble-averaged wave-particle energy transfer data. This method complements existing stellarator Alfven stability calculations that are done in the frequency domain [11] and is currently being benchmarked against results from such existing codes.

### 3. Shear Alfvén - Sound Wave Coupling

Recent experimental results on stellarators (with very low shear ι profiles)[19, 6] and tokamaks (with reversed shear q-profiles) [12] have identified regimes that differ from predictions based on the conventional low β shear Alfvén model, as for example, described in section 2. These typically occur in tokamaks with time-varying q profiles. The shear Alfvén model would predict that as q(r) passes through nearby rational values and drives the lowest continuum frequency to zero, the mode frequency should also pass through zero. However, observations have indicated that the frequency only decreases to some finite plateau value. Likewise in low-shear stellarators, such as HSX [6], low-frequency coherent modes have been observed for $\iota \approx 1.05$ that are near or below the minimum of the lowest Alfvén continuum and would be suggestive of Global Alfvén eigenmodes (GAE). However, when the rotational transform is varied, the mode frequency does not change as expected. Measurements indicate that the dominant poloidal number m is odd and that it is greater than 1 making the parallel wavenumber (and hence mode frequency) too large to match experiment [18].

These observations have motivated the inclusion of the parallel compressibility or finite temperature effects into the mode analysis. In addition to the shear Alfvén mode, acoustic, geodesic acoustic and coupled acoustic-shear Alfvén modes are considered. The compressibility effects are expected to establish a minimum frequency of the Alfvénic mode. In addition, for a given mode frequency, sound waves would have much larger $k_{//}$ than Alfvénic modes, making them insensitive to iota scaling. Temperature effects have been introduced for the case of down-sweeping modes in tokamaks [13] and explored analytically for stellarators [14]. The STELLGAP code [15] has recently been generalized to solve the following coupled set of equations that include Alfvénic modes, sound waves, and their coupling:

$$-\omega^2 g\eta - \mathrm{v}_A^2(\mathbf{B}\bullet\nabla)\frac{g}{B^2}(\mathbf{B}\bullet\nabla)\eta = C_s^2B^2\left[(\mathbf{B}\bullet\nabla)\zeta - \eta G\right]G$$

$$-\omega^2 B^2\zeta - C_s^2(\mathbf{B}\bullet\nabla)(\mathbf{B}\bullet\nabla)\zeta = -C_s^2(\mathbf{B}\bullet\nabla)(\eta G) \qquad (2)$$

Here $g = \nabla\rho\bullet\nabla\rho$, $G = \nabla\rho\bullet\nabla\times\left(\mathbf{B}/B^2\right)$, $C_s^2 = \gamma Z\,kT_e/M_i$, ρ = flux surface label. Setting the left-hand side terms in the first equation to zero leads to the conventional shear Alfvén continuum equation, as previously solved in STELLGAP. These equations can be shown to be equivalent to those derived earlier by Fesenyuk [16] by making a change of variables and taking the low β limit. These are surface equations and eigenvalues and eigenmodes of this system are obtained for each flux surface through making Fourier expansions of the η and ζ functions in poloidal/toroidal angles; equilibrium data is obtained from the VMEC code and transformed into magnetic straight-field line coordinates for the coefficients. Applying both this model and the earlier uncoupled shear Alfvén model to the HSX experiment leads to the

following continuum plots for the n = 1 mode family.

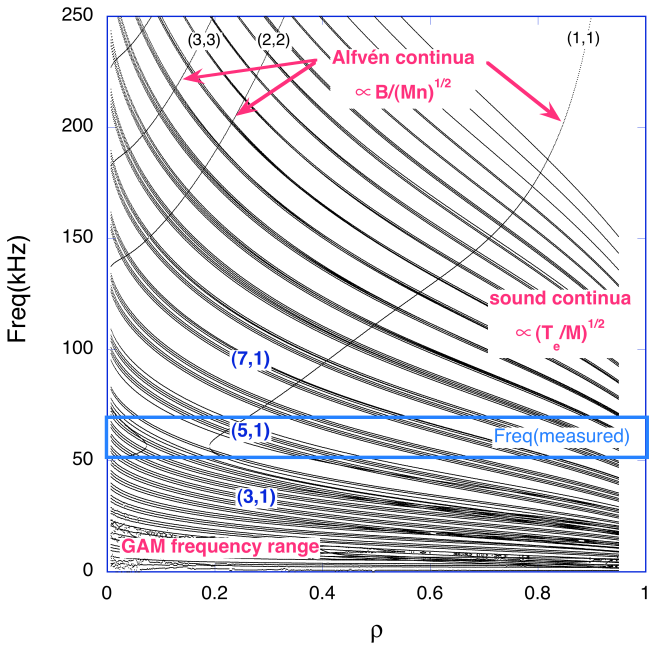


*Figure 3 – Coupled Alfvén/sound continua for n = 1 mode family in HSX.*

Fig. 3 shows the continua predicted by Eq. (2) using the HSX equilibrium and the n = 1 mode family, where the sideband modes n = -5, -4, -3, -1, 0, 3, 4, 5; with m = 0 to 10 for each n, have been used. Roots are found at frequencies 5 - 10 kHz, corresponding to n = 0 modes, which are GAM's (geodesic acoustic modes) that were introduced in [17] and are thought to play an important role in the development of zonal flows. Couplings can occur between shear Alfvén and sound continua when their frequencies are similar; however, for this figure we have not attempted to include the spectrum of modes required to resolve all of the couplings of this type that can be present in this frequency range. The measured modes in HSX are global with amplitudes peaking at $\rho \sim 0.3 - 0.4$. The lowest shear Alfvén continuum (m=1,n=1) that results from including sound wave coupling is also shown. The Alfvén continuum for m=3, n=1 would be at much higher frequency, ~2 MHz. Over the plasma region where the mode amplitude peaks, sound waves with n=1, m=3, 5 and 7 represent a reasonably good match to the measured mode frequencies. Frequency mismatches can likely be accounted for by a small intrinsic radial electric field, which is unknown. Since the variation in the acoustic mode frequency with radius is significantly smaller than that for the Alfvénic mode, global structures are more likely to exist for the former due to reduced phase mixing. It is also observed on HSX that the mode amplitude is very sensitive to magnetic ripple, introduced when quasi-symmetry is broken. This observation supports the conjecture that the excited mode is predominantly acoustic, since the electron drive for the acoustic mode should be more sensitive to ripple (by factor $\beta^{-1}$) than the drive for Alfvenic modes [18]. HSX plasmas are generated and heated by ECRH, therefore, the ions are cold and do not Landau damp acoustic modes. Based on these results, the acoustic mode seems to be the most likely candidate to explain the instability observed on HSX. Sound wave/compressibility effects and GAM couplings are also thought to be of importance in explaining the lower frequency limits on time-varying modes seen in reversed shear regimes in LHD [19].

## 4. Field Ripple Analysis for ITER and finite β effects

Tokamaks experience small symmetry-breaking field errors from a variety of sources, such as discrete toroidal coils, instability-related control coils and ferritic materials. In future devices such as ITER, DEMO and reactors, the use of ferritic steels, in particular, is expected to be quite significant, due to their superior neutron damage and heat loading characteristics. For these reasons, it is important to model such tokamaks as three-dimensional devices; the tools developed for stellarator modeling are applicable for this purpose. Symmetry-breaking effects can degrade energetic particle confinement as they break the invariance of the toroidal canonical momentum; they can also alter Alfvénic mode behavior and the associated turbulent transport since the field errors in the plasma can be of a similar wavelength and magnitude as the turbulent magnetic fields. The starting point for analyzing these effects is in the equilibrium calculation.

The VMEC 3D equilibrium code [20] operated in free boundary mode has been used in conjunction with external magnetic field data to calculate rippled equilibria for ITER. The external magnetic field data was provided in Ref. [21] and includes the effects of TF ripple, ferritic inserts, and tritium blanket modules (TBM); these were evaluated using the ANSYS code. A code was developed to interpolate this data onto the cylindrical coordinates grid that VMEC uses, Fourier transform with respect to the toroidal angle, and incorporate this data into VMEC's external field (mgrid) file. A set of discrete filamentary poloidal field coils were also included in the external field, and by varying the currents in these coils, the ITER outer flux surface shape could be matched. Examples of ripple levels internal to the plasma are displayed in Fig. 4. Here, color contours of ripple, defined by $(B_{max} - B_{min})/ (B_{max} + B_{min})$ are plotted, where the maxima and minima are evaluated at constant flux surface location and poloidal angle. The three cases shown are for (a) TF ripple + ferritic inserts, (b) TF ripple + ferritic inserts + 3 TBM's located at toroidal angles of 0°, 120°, and 240°, and (c) TF ripple + ferritic inserts + 3 TBM's located at toroidal angles of -40°, 0°, and 40°. As can be seen, ripple levels rise with the inclusion of the TBM's. Also, placing the TBM's equidistantly around the torus [case(b)] significantly reduces the ripple level and its extent into the plasma as compared to the case(c) where the TBM's are on one side of the plasma.

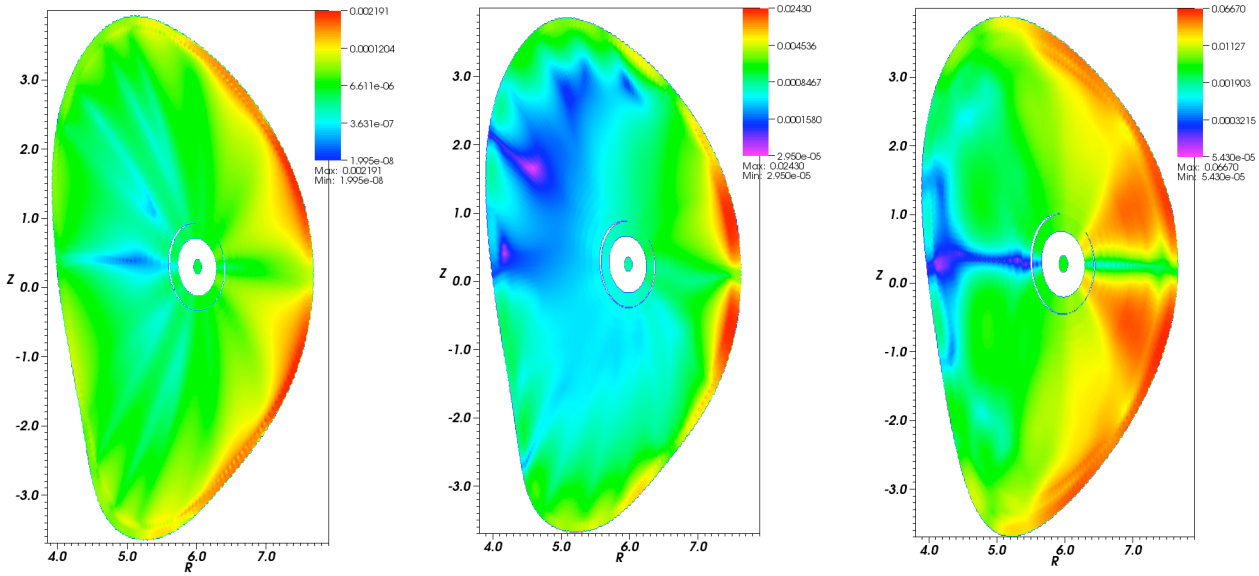


*Figure 4 – ITER ripple contours in R-Z plane for: (a) toroidal field (TF) coil and ferritic insert effects only; (b) same as (a), but with 3 TBM's added at $\phi$ = 0°, 120°, 240°; (c) same as (a), but with 3 TBM's added at $\phi$ = -40°, 0°, 40°.*

This data can be condensed further if only the maximum ripple on each surface is plotted. Such a plot is given in Fig. 5(a) and again illustrates the strong increases in ripple with the inclusion of the TBM's and especially the high ripple levels associated with placing the TBM's together in the -40°, 0°, and 40° configuration. It should be noted that these plots do not show the fact that the ripple components from the TF coils and ferritic inserts are dominated by relatively high toroidal mode numbers (n = 18) while those from the TBM's are n = 1 [for case (c)] or n = 3 [for case(b)].

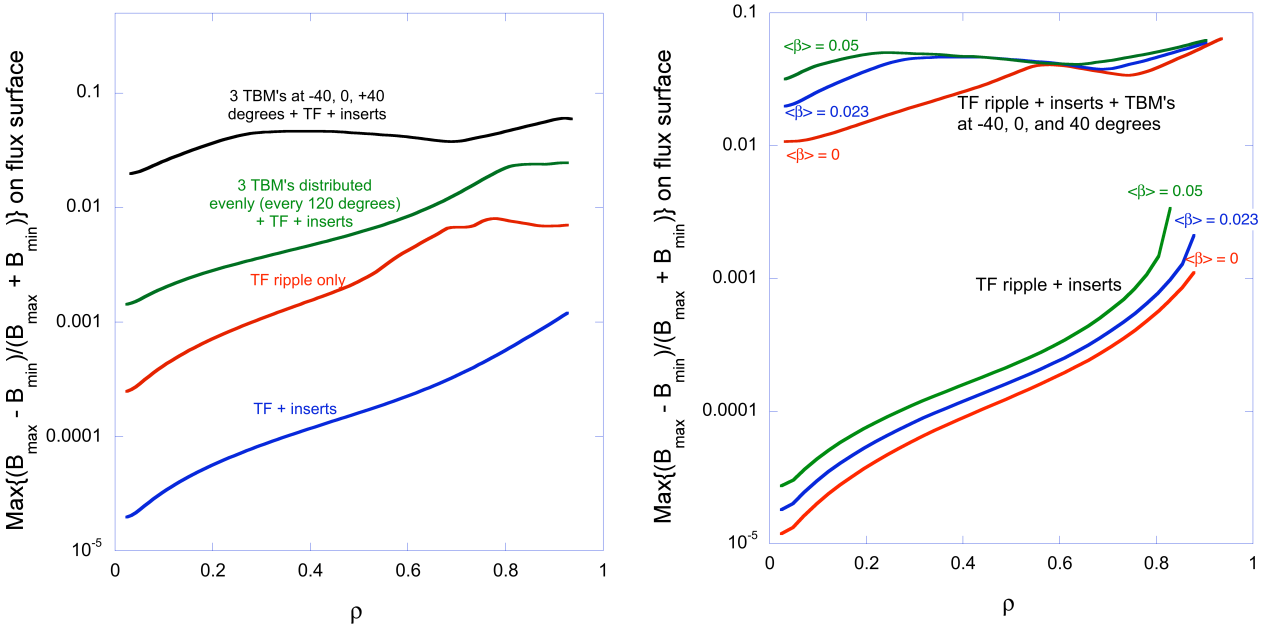


*Figure 5 – (a) Radial variation of maximum ripple in ITER for different configurations; (b) radial variation of ripple in ITER for as a function of equilibrium <β> for two configurations.*

One of the primary reasons for using the VMEC 3D equilibrium calculation instead of simply adding the vacuum ripple fields to an axisymmetric equilibrium is to evaluate the effects of the finite Shafranov shift, diamagnetic currents and Pfirsch-Schlüter currents on the internal ripple levels. Previous work on these effects [22, 23] has been reported for the case of circular tokamaks. The data shown in Figs. 4(a)-(c) and 5(a) is based on an equilibrium with <β> = 0.023. In Fig. 5(b) the effects of raising and lowering β are displayed. As indicated, the plasma generally acts to amplify internal ripple levels. This is especially apparent for the low n ripple caused by the TBM's (which remains finite further into the plasma), but is also present for the n = 18 ripple of the TF coils and ferritic inserts.

## 5. Conclusions

Energetic particle stability and confinement issues are of primary importance for stellarators and rippled tokamaks due to the desirability of maintaining high heating efficiencies and avoiding localized first wall damage. In the case of stellarators the complex magnetic field structure leads to higher mode coupling and more degrees of freedom in Alfvén spectrum. Although many of the experimental observations of these modes have been from the lower frequency gaps (TAE, GAE, RSAE) that are shared in common with the axisymmetric tokamak, the non-symmetric field components play a role in setting the mode structure and introducing new higher frequency gaps. This paper has shown that these effects can be taken into account and that modes with global radial mode structure remain present and can be readily identified and connected, for example, with experimental observations in the LHD

device. For lower frequency modes below the minima in the lowest Alfvén continuum, it has been demonstrated that the sound wave continuum occurs and is relevant to regimes on the HSX stellarator where coherent activity has been observed. Future tokamaks, such as ITER will have to take into account the effects of new field ripple components caused by ferritic structures near the plasma. A method has been developed for including these effects in the 3D VMEC equilibrium code. This has allowed an evaluation of ripple levels within the plasma, taking into account the effects of plasma diamagnetic currents, the Shafranov shift and Pfirsh-Schlüter currents. It is found that such effects can amplify ripple levels over what is predicted from vacuum field calculations. This will likely require installation of external correction coils to compensate the field perturbations from of the ferritic materials in order to avoid enhanced alpha losses.

**Acknowledgements** – Research sponsored by the U.S. Department of Energy under Contract DE-AC05-00OR22725 with UT-Battelle, LLC. Helpful assistance from Steven Hirshman in the use of the free-boundary VMEC code is gratefully acknowledged.

[1] WELLER, A., SPONG, D. A., JAENICKE, R., et al., Phys. Rev. Lett. **72**, 1220 (1994).
[2] ISOBE, M., TOI, K., MATSUSHITA, H., et al. Nucl. Fusion **46**, S918 (2006).
[3] TOI, K., YAMAMOTO, S., NAKAJIMA, N., et al. Plasma Phys. and Control. Fusion **46**, S1 (2004).
[4] JIMENEZ-GOMEZ, R., ASCASIBAR, E., et al., Fusion Science and Technology **51**, 20 (2007).
[5] YAMAMOTO, S., NAGASAKI, K., SUZUKI, Y., et al., Fusion Science and Technology, **51**, 92 (2007).
[6] DENG, C., BROWER, D.L., DING, W.X., et al.,14th International Stellarator Workshop, Greifswald, Germany (2003).
[7] SPONG, D. A., TODO, Y., 49th Annual Meeting of the Division of Plasma Physics (12-16 November 2007, Orlando), PP8.00098.
[8] NÜHRENBERG, C., Phys. of Plasmas **6**, 137 (1999).
[9] OSAKABE, M., *et al.*, Nucl. Fusion **46**, S911 (2006).
[10] TODO, Y., NAKAJIMA, N., OSAKABE, M., YAMAMOTO, S., SPONG, D. A., Plasma Fusion Res. **3**, S1074 (2008).
[11] KONIES, A., Phys. of Plasmas **7**, 1139 (2000).
[12] SHARAPOV, S. E., ALPER, B., BERK, H. L., et al., Phys. Plasmas **9**, 2027 (2002).
[13] BREIZMAN, B. N., BERK, H. L., PEKKER, M. S., et al., Phys. of Plasmas **10**, 3649 (2003).
[14] KOLESNICHENKO, YA. I., LUTSENKO, V. V., et al., Phys. of Plasmas **14**, 102504 (2007).
[15] SPONG, D. A., SANCHEZ, R., WELLER, A., Phys. of Plasmas **10**, 3217 (2003).
[16] FESENYUK, O. P., KOLESNICHENKO, YA. I., WOBIG, H., et al., **9**, 1589 (2002).
[17] WINDSOR, N., JOHNSON, J. L., DAWSON, J. M., Phys. Fluids **11**, 2448 (1968).
[18] DENG, C.B., BROWER, D.L., SPONG, D.A., BREIZMAN, B.N., et al., manuscript in preparation (2008).
[19] TOI, K., WATANABE, F.. TOKUZAWA, T., et al., 10th IAEA TM on Energetic Particles in Magnetic Confinement Systems, 8-10 Oct., 2007, Kloster Seeon, Germany.
[20] HIRSHMAN, S. P., WHITSON, J. C., Phys. Fluids **26**, 3553 (1983).
[21] SABIENE, G., personal communication (2007) and CALCOLI, L.T., ROCHELLA, M., Ripple reduction using SS430 Fe inserts, Frascati (2007).
[22] SUZUKI, Y., NAKAMURA, Y., KONDO, K. Nucl. Fusion **43**, 406 (2003).
[23] JOHNSON, J. L., REIMAN, A. H., Nucl. Fusion **38**, 1116 (1988).